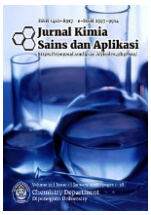
ISSN: 1410-8917
Jurnal Kimia Sains & Aplikasi
e-ISSN: 2597-9914

Jurnal Kimia Sains dan Aplikasi 29 (1) (2026): 1-9

Jurnal Kimia Sains dan Aplikasi
Journal of Scientific and Applied Chemistry

Journal homepage: http://ejournal.undip.ac.id/index.php/ksa



Determination of Kinetic and Thermodynamic Parameters of Pb(II) Ion Adsorption Using Dithizone-Immobilized Coal Fly Ash

Muh Rizal B. [1,*], Mudasir Mudasir [2], Dwi Siswanta [2], Melvi Muharmi [3], Vebria Ardina [4], Teguh Setyawan [3], Nur Jaya [3], Defia Indah Permatasari [1], Revi Maylina Tanjung [3]

[1] Department of Chemistry, Faculty of Sciences and Technology, Universitas Jambi, Jambi, Indonesia
[2] Department of Chemistry, Faculty of Mathematics and Natural Sciences, Universitas Gadjah Mada, Yogyakarta, Indonesia
[3] Department of Analytical Chemistry, Faculty of Sciences and Technology, Universitas Jambi, Jambi, Indonesia
[4] Department of Industrial Chemistry, Faculty of Sciences and Technology, Universitas Jambi, Jambi, Indonesia

* Corresponding author: muh.rizal@unja.ac.id

https://doi.org/10.14710/jksa.29.1.1-9

Article Info

Article history:

Received: 29th June 2025
Revised: 03rd November 2025
Accepted: 18th December 2025
Online: 07th February 2026

Keywords:
Adsorption; Kinetics; Pb(II); Thermodynamics

Abstract

The immobilization of dithizone on the surface of coal fly ash was successfully achieved, as evidenced by Fourier-transform infrared (FT-IR) and X-ray diffraction (XRD) characterization. The dithizone-immobilized coal fly ash (CFA-Dzt) was then used for Pb(II) ion adsorption. The parameters studied included the effects of pH, kinetics, and thermodynamics on Pb(II) ion adsorption using a batch experimental system. The results showed that the optimum pH for Pb(II) adsorption using CFA-Dzt was 5. The adsorption kinetics of Pb(II) ions followed the pseudo-second-order kinetic model, with an adsorption activation energy of 27.280 kJ mol^{-1}. The Langmuir isotherm model best described the adsorption behavior, with a maximum adsorption capacity of 34.13 mg g^{-1}. Thermodynamic analysis revealed Gibbs free energy changes ($\Delta G°$) of −24.630, −25.850, −26.810, and −28.550 kJ mol^{-1} at 293, 303, 313, and 323 K, respectively. The enthalpy change ($\Delta H°$) of the adsorption at this temperature range was +12.770 kJ mol^{-1}, indicating that Pb(II) ion adsorption on the adsorbent is an endothermic process, and its entropy change ($\Delta S°$) was +127.290 J mol^{-1}, suggesting that the adsorption of Pb(II) ion on CFA-Dzt is dominantly driven by the entropic factor.

1. Introduction

The industrial world is currently developing rapidly, producing valuable products while also impacting the environment. Most industries generate waste in the form of solid, liquid, or air pollutants. Liquid waste produced in the mining, paint, and battery manufacturing industries is usually contaminated with heavy metals such as Pb, Cd, Hg, Zn, Ni, and As. These heavy metals significantly contribute to environmental pollution due to their toxic, mutagenic, and carcinogenic effects on living organisms. Almost all heavy metals are toxic, and some, such as mercury, cadmium, and lead, are considered the most dangerous toxins for living organisms and the environment [1, 2].

Heavy metals such as lead (Pb) are major pollutants in the environment because they are non-biodegradable and easily accumulate, posing a threat to public health and environmental degradation [3]. The high solubility of heavy metals in water allows them to be absorbed by living organisms such as plants through their roots and vegetative organs, and can also accumulate in animals such as clams, oysters, shrimp, lobsters, and fish [4]. If these metals enter the human body through the food chain, they can cause health issues such as hemoglobin biosynthesis, increased blood pressure, kidney, brain, and nervous system damage, miscarriages, and behavioral disorders in children, such as aggression, impulsive behavior, and hyperactivity [5]. Therefore, before wastewater is discharged into the environment, it must be treated to reduce or eliminate heavy metals.

Various methods have been employed to remove Pb(II) ions from water, including electrocoagulation, electrodialysis, electrodeposition, electrochemical techniques, photocatalytic processes, membrane filtration, adsorption, and biological treatment [6].

Among these methods, adsorption using modified natural-material-based adsorbents is among the most effective and economical. The primary adsorbents used can include nano-silica-based materials [7], activated carbon composites [8], Magnetic-chitosan composite materials [9], modified zeolites [10], functionalized biochar [11], and modified coal fly ash with chelating ligands such as dithizone [12].

The use of coal fly ash as an adsorbent is considered quite adequate for the adsorption of various metals due to its high efficiency, cost-effectiveness, and ease of availability. Fly ash is a byproduct of coal combustion, accounting for approximately 60–88% of the total coal combustion residue [13]. Fly ash can be used as an adsorbent due to its content of silica, alumina, and unburned carbon. Coal fly ash can also be used as a precursor for the synthesis of porous materials such as silica, zeolite, or activated carbon [14]. Adsorption will be more effective and efficient if coal fly ash is activated first. Activation can be done physically, such as by heating fly ash at high temperatures, or chemically by extracting fly ash using HCl and NaOH [15, 16, 17]. The surface of activated coal fly ash can be further immobilized or modified by hydrophilic or hydrophobic groups to fully activate the surface and enhance its interaction with polar and non-polar pollutants [18].

Activated adsorbents can be immobilized using organic ligands such as dithizone, which acts as a sensitive and selective chelating agent due to its multiple N donor atoms and –NH and –SH electron-donating groups, enabling chelate formation with heavy metal ions such as Pb, Cd, and Hg [12, 19, 20]. n this study, adsorbents based on natural materials, specifically coal fly ash, were developed; however, fly ash has limitations, particularly low adsorption capacity, necessitating surface modification. Since Pb^{2+} ions are soft acids, the adsorbent surface was modified with soft base functional groups such as –SH. Dithizone, with its active –NH and –SH groups, is therefore effective for enhancing Pb^{2+} adsorption. This work focuses on adsorption kinetics, including activation energy, and thermodynamic parameters such as the Gibbs free energy change ($\Delta G°$), enthalpy change ($\Delta H°$), and entropy change ($\Delta S°$).

2. Experimental

2.1. Materials

Caol fly ash (CFA) was obtained from PT. Petrokimia Gresik, dithizone or 1,5-diphenylthiocarbazone, hydrogen chloride (HCl), Sodium hydroxide (NaOH), toluene, lead (II) nitrate ($Pb(NO_3)_2$), and distilled water. All chemicals were obtained from Sigma-Aldrich, and the solvent was ACS Reagent Chemicals, both with purities>99%. They were used directly without further purification.

2.2. Preparation of Adsorbent and Characterization

Before activation, CFA was dried at 100°C for 3 hours, then sieved through a 150-mesh sieve. CFA was activated by refluxing 10 g of CFA with 60 mL of 6M HCl solution at 120°C for 6 hours. The CFA-activated HCl (CFA-HCl) was then neutralized with DI water. Immobilization of dithizone on CFA-HCl was carried out by mixing 8 g of CFA-HCl with 2 g of dithizone in 120 mL of toluene and stirring with a magnetic stirrer at 50°C for 16 hours. The obtained dithizone-immobilized coal fly ash (CFA-Dzt) was then filtered and washed successively with toluene, ethanol, and aquabides solutions until the filtrate showed no remaining dithizone characteristics. The CFA-Dzt solid was then dried at 40°C for 5 hours. The success of dithizone immobilization on the CFA surface was confirmed by Fourier-transform infrared (FT-IR, Shimadzu model FR-IR Prestige 21) and X-ray diffraction (XRD, Bruker AXS D8 Advance Eco) analysis.

2.3. Adsorption Study of Pb(II) Ion

2.3.1. Effect of pH

A total of 20 mg of CFA-Dzt was reacted with 20 mL of 10 ppm Pb(II) ion solution, whose pH was adjusted using HCl and NaOH solutions. The pH range studied was pH 3–9. The adsorption process was carried out in a batch system at room temperature for 60 minutes. After the adsorption process was completed, the Pb(II) ion content in the filtrate was determined using an atomic absorption spectrophotometer (AAS, Perkin Elmer 3110). All experiments were performed in triplicate. The adsorption amount (q_e, mg of Pb(II) g^{-1}) was determined using Equation 1.

$$q_e = (C_o - C_e)\frac{V}{m} \quad (1)$$

Where, C_o and C_e are initial and equilibrium concentrations of Pb(II) (mg L^{-1}), respectively, and V and m are the volume of the aqueous Pb(II) solution (L) and dosage of adsorbent (g), respectively.

2.3.2. Determination of Kinetic Parameters

A total of 20 mg of CFA-Dzt was reacted with 20 mL of a 10 ppm Pb(II) solution at the pH optimum condition. The contact times used were 5, 15, 25, 35, 45, 60, 70, and 100 minutes. The variation in contact time for adsorption was carried out at 293, 303, 313, and 323 K. The data were then fitted with pseudo-first (Equation 2) and second-order (Equation 3) reaction kinetic models [21, 22].

$$\ln(q_e - q_t) = \ln q_e - \ln k_1 t \quad (2)$$

q_t and q_e are the amounts of Pb(II) ions adsorbed at time t and at equilibrium (mg g^{-1}), and k_1 is the pseudo-first-order rate constant (min^{-1}). By plotting ln (q_e-q_t) vs t, the value of k_1 can be obtained from the slope of the line equation.

$$\frac{t}{q_t} = \frac{1}{k_2 q_e^2} + \frac{1}{q_e} t \quad (3)$$

By plotting t/q_t against t, a linear relationship was obtained, allowing the determination of q_e and the pseudo-second-order rate constant k_2 from the slope and intercept, respectively.

Activation energy (Ea) is an important parameter in adsorption kinetics studies, obtained from a plot of the adsorption rate (k) versus temperature (T). The activation energy was determined from the temperature dependence of k using the Arrhenius equation (Equation 4).

$$\ln k = \ln A - \frac{Ea}{RT} \quad (4)$$

k is the adsorption rate constant, A is the collision frequency factor, R is the universal gas constant (8.314 J $mol^{-1}K^{-1}$), and T is the temperature (K). A linear relationship was obtained by plotting ln k versus $1/T$, and the activation energy was calculated from the slope of the resulting straight line [19, 23].

2.3.3. Determination of Thermodynamic Parameters

A total of 20 mg of CFA-Dzt was reacted with 20 mL of Pb(II) ion solutions at different concentrations (10, 20, 30, 40, 50, 75, and 100 ppm) at the pH optimum condition. The adsorption process lasted 60 minutes at 293, 303, 313, and 323 K. The isotherm models tested in this study were the Langmuir isotherm model (Equation 5), the Freundlich (Equation 6), and the Temkin (Equation 7) [24, 25, 26].

$$\frac{C_e}{q_e} = \frac{C_e}{q_m} + \frac{1}{q_m K_l} \quad (5)$$

q_e is the amount of solute absorbed on the sorbent surface (mg g^{-1}), C_e is the ion concentration in the solution (mg L^{-1}), q_m is the maximum adsorption capacity (mg g^{-1}), and K_l is the Langmuir adsorption constant (L mg^{-1}).

$$\log q_e = \log K_F + \frac{1}{n} \log C_e \quad (6)$$

K_F (mg g^{-1}) is the Freundlich constant that indicates the adsorption capacity of the adsorbent and the strength of the relationship between the adsorbate and the adsorbent. The K_F value is obtained from the intercept plot between log q_e vs log C_e. The adsorption intensity value (n) is obtained from the slope of the graph.

$$q_e = \frac{RT}{b_T} \ln A_T + \frac{RT}{b_T} \ln C_e \quad (7)$$

Where, R (8.314 J mol^{-1} K^{-1}) is the universal gas constant, T (K) is the temperature, and C_e (mmol L^{-1}) is the equilibrium concentration of metal ions. b_T (kJ mol^{-1}) is the Temkin constant related to the heat of adsorption, and K_T (L g^{-1}) is the Temkin isothermal equilibrium constant. The values of the Temkin isothermal equilibrium constant (K_T) and Temkin adsorption energy (b_T) are obtained from the plot of q_e versus ln C_e. The slope of the curve is $\frac{RT}{b_T}$, and the value of K_T is obtained from the intercept.

Adsorption thermodynamic parameters such as $\Delta G°$ are obtained from (Equation 8), while $\Delta H°$ and $\Delta S°$ are obtained from the Van't Hoff equation (Equation 9).

$$\Delta G°_{ad} = -RT \ln K \quad (8)$$

$$\ln K = \frac{\Delta S°}{R} - \frac{\Delta H°}{R} \frac{1}{T} \quad (9)$$

The values of $\Delta H°$ and $\Delta S°$ can be determined by plotting ln K versus $1/T$. The slope can be used to determine the value of $\Delta H°$, and $\Delta S°$ can be determined from the intercept. The relationship between $\Delta G°$, $\Delta H°$, and $\Delta S°$ was obtained according to Equation 10, following the principles of the venerable thermodynamic law [24, 27].

$$\Delta G° = \Delta H° - T\Delta S° \quad (10)$$

3. Results and Discussion

3.1. Characterization of Dithizone-Immobilized Coal Fly Ash (CFA-Dzt)

The success of dithizone immobilization on CFA surfaces can be demonstrated by FTIR characterization, specifically by comparing the spectra before and after immobilization. Figure 1a shows that CFA-Dtz exhibits characteristic absorption peaks similar to those of dithizone. These characteristics are observed at wavenumbers 1141 and 1219 cm^{-1}, which correspond to C=S absorption peaks; 1319 cm^{-1} is a characteristic peak of C-N; 1435 cm^{-1} is the stretching vibration of C=C; and the N=N bond vibration at 1496 cm^{-1}. These characteristic peaks are not found in the coal fly ash before (CFA) and after activation (CFA-HCl). The appearance of these characteristic peaks indicates that dithizone has been successfully immobilized on the dithizone surface.

XRD analysis was conducted to support the FTIR results. As shown in Figure 1b, CFA-Dtz displays new diffraction peaks at 2θ of 37°, 44°, 64°, and 77°, which are characteristic of dithizone. Meanwhile, the dominant phases of coal fly ash remain quartz (Q) and mullite (M), as indicated by peaks at 2θ around 21°, 26°, 36°, 50°, and 68° [28].

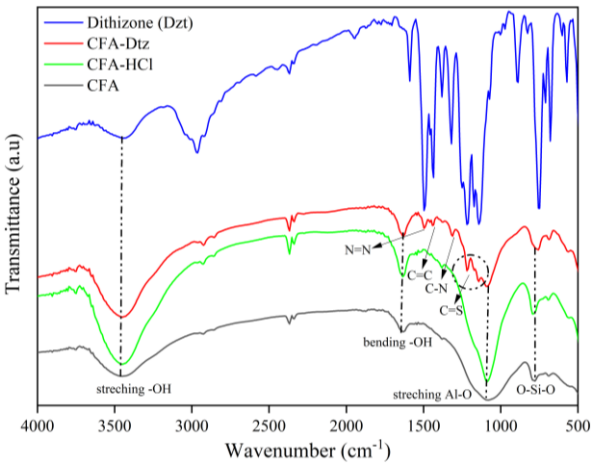


Figure 1. FTIR spectra of CFA, CFA-HCl, CFA-Dtz, and Dithizone

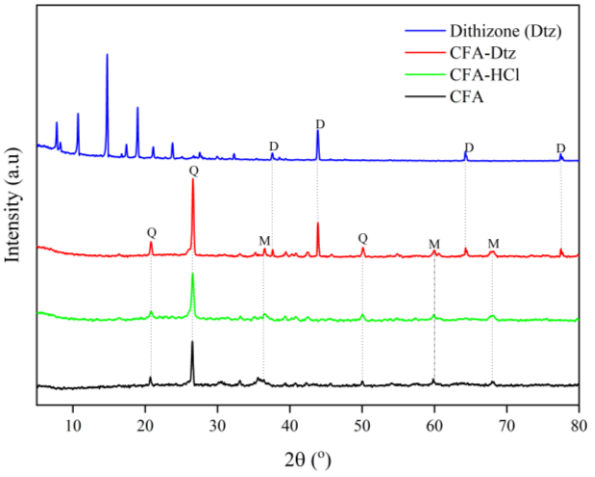


Figure 2. XRD pattern of CFA, CFA-HCl, CFA-Dtz, and Dithizone

Table 1. Adsorption kinetics model at various temperatures

Kinetic model	Parameters	Temperature (K)			
		293	303	313	323
Pseudo-first-order	R^2	0.7844	0.1544	0.0791	0.0125
	q_{max} (mg g^{-1})	1.373	0.993	0.749	0.658
	h (mg $g^{-1}min^{-1}$)	8.37×10^{-3}	6.75×10^{-3}	4.94×10^{-3}	1.05×10^{-3}
	k_1 (min^{-1})	6.10×10^{-3}	6.80×10^{-3}	6.60×10^{-3}	1.60×10^{-3}
Pseudo-second-order	R^2	0.9929	0.9978	0.9988	0.9975
	q_{max} (mg g^{-1})	8.540	8.865	9.033	9.259
	h (mg $g^{-1}min^{-1}$)	5.450	7.974	10.288	19.048
	k_2 (g mg^{-1} min^{-1})	0.75×10^{-1}	1.01×10^{-1}	1.26×10^{-1}	2.2×10^{-1}

3.2. Effect of pH on Pb(II) Adsorption

The pH of a solution is an important factor in the adsorption process. The pH of a solution can affect the surface charge of the adsorbent and the speciation of Pb(II) metal ions in the solution. The speciation of Pb(II) ions in a solution is greatly influenced by the conditions of the solution. Under acidic conditions, the speciation of Pb(II) ions can take the form of Pb^{2+} and $PbNO^{3+}$, while under basic conditions, hydroxide species of lead may form, such as $Pb(OH)^+$, $Pb(OH)_2$, $Pb(OH)_3^-$, $Pb_2(OH)_3^+$, $Pb_3(OH)_4^+$, and $Pb_4(OH)_4^{4+}$. Because these distinct species interact differently with the adsorbent's active sites, determining the optimum pH is essential for maximizing adsorption effectiveness [29, 30].

The effect of solution pH on Pb(II) adsorption was investigated over a pH range of 3–9, as shown in Figure 3. The adsorption capacity increased with increasing pH up to an optimum value, after which it decreased at higher pH levels. The maximum adsorption occurred at pH 5. This behavior can be attributed to the predominance of Pb^{2+} ions in solution at this pH, which enhances electrostatic interactions between the positively charged Pb^{2+} ions and the negatively charged active sites of the adsorbent. At pH values around 5.21, Pb^{2+} is the dominant species in $Pb(NO_3)_2$ solution, leading to more efficient adsorption. These results are consistent with previously reported findings [31].

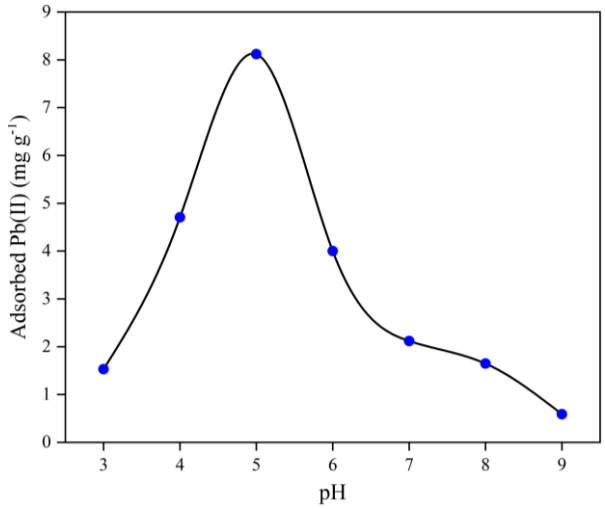


Figure 3. The effect of pH on the adsorption of Pb(II) ions

3.3. Kinetic and Activation Energy Evaluation for Pb(II) Adsorption

Kinetic parameters were studied by varying the contact time at temperatures between 293 and 323 K. The time required to reach adsorption equilibrium reflects the adsorption rate and the interaction dynamics between the adsorbent and Pb(II) ions. Once equilibrium is achieved, further increases in contact time do not result in a significant increase in the amount of Pb(II) adsorbed. The effect of contact time on Pb(II) adsorption at different temperatures is presented in Figure 4a. Figure 4a generally shows that: (i) at a given temperature, adsorption capacity increases with contact time due to prolonged interaction between the adsorbent and adsorbate, and (ii) at the same contact time, higher temperatures result in greater Pb(II) adsorption capacity. This is attributed to increased kinetic energy of the adsorbate at higher temperatures, which enhances molecular mobility and collision frequency with active sites on the adsorbent surface, leading to higher adsorption [32].

The adsorption kinetics of Pb(II) ions onto CFA-Dzt were investigated using pseudo-first-order and pseudo-second-order kinetic models at temperatures of 293, 303, 313, and 323 K, with the calculated kinetic parameters listed in Table 1. As shown in Table 1, the pseudo-second-order model exhibits significantly higher regression coefficients ($R^2 \geq 0.99$) at all studied temperatures compared to the pseudo-first-order model. This indicates that the adsorption of Pb(II) ions onto CFA-Dzt is better described by the pseudo-second-order kinetic model. The dominance of this model suggests that the adsorption process proceeds through two distinct stages: an initial rapid uptake of Pb(II) ions, followed by a slower adsorption stage as the system approaches equilibrium.

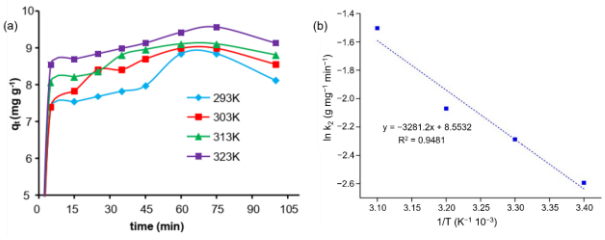


Figure 4. (a) The effect of contact time on the adsorption of Pb(II) ions at various temperatures, (b) graph of the relationship between ln *k* and 1/*T*

Table 1. Adsorption kinetics model at various temperatures

Kinetic model	Parameters	Temperature (K)			
		293	303	313	323
Pseudo-first-order	R^2	0.7844	0.1544	0.0791	0.0125
	q_{max} (mg g^{-1})	1.373	0.993	0.749	0.658
	h (mg $g^{-1}min^{-1}$)	8.37×10^{-3}	6.75×10^{-3}	4.94×10^{-3}	1.05×10^{-3}
	k_1 (min^{-1})	6.10×10^{-3}	6.80×10^{-3}	6.60×10^{-3}	1.60×10^{-3}
Pseudo-second-order	R^2	0.9929	0.9978	0.9988	0.9975
	q_{max} (mg g^{-1})	8.540	8.865	9.033	9.259
	h (mg $g^{-1}min^{-1}$)	5.450	7.974	10.288	19.048
	k_2 (g mg^{-1} min^{-1})	0.75×10^{-1}	1.01×10^{-1}	1.26×10^{-1}	2.2×10^{-1}

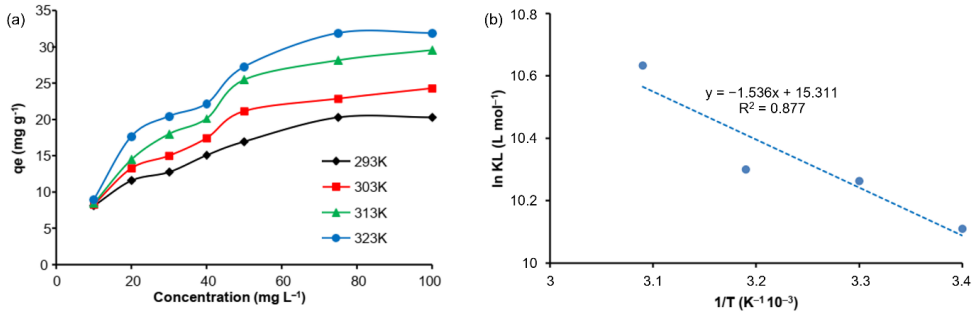


Figure 5. (a) The effect of contact time on the adsorption of Pb(II) ions at various temperatures, (b) graph of the relationship between ln K_l and $1/T$

Table 1 shows that the pseudo-second-order kinetic model, tested at various temperatures, yields higher regression coefficients ($R^2 \geq 0.99$) than the pseudo-first-order model. Thus, it can be concluded that the adsorption kinetics of Pb(II) ions by CFA-Dtz for various temperatures studied follow the pseudo-second-order kinetic model. Increasing the adsorption temperature also increases the maximum adsorption capacity (q_{max}), the initial adsorption rate (h), and the adsorption rate constant (k), as shown in Table 1. The pseudo-second-order kinetic model implies that the adsorption process occurs in two stages: the first stage involves rapid adsorption of the adsorbate in the initial minutes, followed by a much slower stage before equilibrium is reached, as shown in Figure 4a.

The k values obtained at various temperatures were then used to determine the adsorption activation energy using the Arrhenius equation (Equation 4). The adsorption activation energy is obtained by plotting a graph of ln k versus $1/T$, as shown in Figure 4b. The slope value of the graph is used to determine the Ea value. From the Arrhenius equation, the slope is $\frac{Ea}{RT}$ where R is the universal gas constant (8.314 J $mol^{-1}K^{-1}$). By substituting the slope value from the linear equation, the adsorption activation energy is obtained as 27.280 kJ mol^{-1}. The adsorption activation energy is the minimum energy required for an adsorbate to interact with the active sites on the adsorbent surface. Thus, in the adsorption process of Pb(II) ions by CFA-Dtz, a minimum energy of 27.280 kJ is required for each mole of adsorbate to bind or interact with the active sites on the adsorbent surface.

3.4. Determination of Isotherm and Thermodynamic Parameters for Pb(II) Adsorption

The adsorption isotherm model describes the relationship between the concentration of the adsorbate and the amount of substance adsorbed on the adsorbent surface [33]. The adsorption isotherms studied in this research are the Freundlich, Langmuir, and Temkin isotherm models. The adsorption isotherm study was conducted by measuring the adsorption data of Pb(II) ions at varying initial concentrations of Pb(II) ions. The concentration variations used in this study were 10–100 ppm, where the adsorption process was carried out at temperatures of 293-323 K, as shown in Figure 5a.

Figure 5a implicitly explains that: (i) at a constant temperature, an increase in the concentration of Pb(II) ions is followed by an increase in its adsorption capacity. This is because at higher concentrations, the number of Pb(II) ions in the solution increases, resulting in a greater number of Pb(II) ions being adsorbed onto the adsorbent surface, and (ii) at the same concentration, an increase in temperature also increases adsorption capacity. This is because an increase in temperature increases the adsorbate's kinetic energy. This increase in kinetic energy causes the adsorbate molecules to move faster, leading to more frequent collisions between the adsorbate and the adsorbent's active sites, thereby increasing the number of Pb(II) ions adsorbed onto the adsorbent.

Table 2. The model isotherm adsorption of Langmuir, Freundlich, and Temkin

Model isotherm	Parameters	Temperature (K)			
		293	303	313	323
Freundlich	R^2	0.977	0.982	0.982	0.947
	n	3.932	3.501	3.167	3.546
	K_F (mg g^{-1})	6.780	7.438	8.357	10.580
Langmuir	R^2	0.987	0.993	0.990	0.992
	q_m (mg g^{-1})	22.321	26.247	32.258	34.130
	R_L	0.076	0.067	0.065	0.046
	K_l (L mg^{-1})	2.45×10^4	2.86×10^4	2.96×10^4	4.15×10^4
Temkin	R^2	0.931	0.965	0.958	0.961
	B_t (kJ mol^{-1})	0.713	0.584	0.481	0.506
	K_T (L g^{-1})	4.238	3.518	3.264	6.258

Table 3. Comparison of q_{max} Pb(II) adsorption

Adsorbent	Temperature range (K)	q_{max} (mg g^{-1})	Ref.
$MgFe_2O_4$	273–373	7	[34]
Coal bottom ash-Dhitizone	283–313	25.2	[35]
core/shell CdZnS/ZnS	293–393	35.6	[36]
Biochar	298–358	15.22	[37]
PEI@GO membranes	298–328	33.33	[38]
CFA-Dithizone	293–323	34.13	This work

The isotherm analysis results in Table 2 show that the Freundlich, Langmuir, and Temkin models all fit the experimental data well, as indicated by their correlation coefficients (R^2). Among them, the Langmuir model exhibits the highest correlation (R^2 0.99), indicating that Pb(II) adsorption onto CFA-Dzt at all temperatures is best described by the Langmuir isotherm. Based on Table 1, the maximum adsorption capacity increases with increasing adsorption temperature, indicating that the equilibrium shifts toward the product. The R_l value describes the affinity between the adsorbate and the adsorbent. An R_l value >1 indicates an unfavorable isotherm type, R_l<1 indicates a linear pattern, 0<R_l<1 indicates a favorable pattern, and R_l=0 indicates an irreversible pattern. The R_l value in Table 2 decreases with increasing temperature, indicating that higher temperatures decrease the affinity between the adsorbate and adsorbent, as confirmed in Table 3 by a positive $\Delta S°$ value [39].

Table 3 compares the maximum adsorption capacities of Pb(II) ions for different adsorbents over a given temperature range. Based on these data, it can be seen that the use of different adsorbents yields different Pb(II) adsorption capacities, which are influenced by the abundance of active sites in each adsorbent type. The adsorption capacity value of dithizone-immobilized coal fly ash is slightly larger than that of dithizone-immobilized bottom ash.

Table 4. Thermodynamic parameters of Pb(II) ion adsorption

Temperature (K)	ΔG (kJ mol^{-1})	ΔH (kJ mol^{-1})	ΔS (J mol^{-1})
293	-24.630	+12.770	+127.290
303	-25.850		
313	-26.810		
323	-28.550		

The value of $\Delta G°$ is calculated using (Equation 8), while the values of $\Delta H°$ and $\Delta S°$ are calculated from Equation 9 by plotting the relationship between ln K_l and $1/T$, and the value of $\Delta H°$ is obtained from −slope ×R, and $\Delta S°$ is obtained from the intercept ×R. The graph of the relationship between $1/T$ and ln K_l, along with the calculated values of $\Delta G°$, $\Delta H°$, and $\Delta S°$, are presented in Figure 5b and Table 4, respectively.

$\Delta G°$ is a key thermodynamic parameter used to evaluate the spontaneity of an adsorption process. A negative $\Delta G°$ value indicates that the adsorption occurs spontaneously. The enthalpy change ($\Delta H°$) represents the heat involved in adsorption at constant pressure; a negative $\Delta H°$ signifies an exothermic process, whereas a positive $\Delta H°$ indicates an endothermic process. The entropy change ($\Delta S°$) reflects variations in the degree of disorder of the system. A positive $\Delta S°$ value suggests increased randomness at the solid–liquid interface, possibly due to structural rearrangements of the adsorbate and adsorbent. The relationship among these thermodynamic parameters is expressed in Equation (10). When both $\Delta H°$ and $\Delta S°$ are positive, the adsorption process becomes spontaneous ($\Delta G°$ < 0) only when the $T\Delta S°$ term exceeds $\Delta H°$, which typically occurs at higher temperatures [24, 27].

The $\Delta G°$ values listed in Table 4 are negative at all investigated temperatures, confirming that the adsorption of Pb(II) ions onto CFA-Dzt occurs spontaneously. Moreover, the magnitude of $\Delta G°$ becomes increasingly negative with rising temperature, indicating that the adsorption process is thermodynamically more favorable at higher temperatures. The calculated $\Delta H°$ value of +12.770 kJ mol^{-1} suggests that the adsorption

process is endothermic. In addition, the positive $\Delta S°$ value of +127.290 J mol^{-1} K^{-1} indicates an increase in randomness at the solid–liquid interface during adsorption, which may be attributed to structural rearrangements and enhanced mobility of Pb(II) ions with increasing temperature.

4. Conclusion

The adsorption of Pb(II) ions onto CFA-Dzt was optimal at pH 5 and followed a pseudo-second-order kinetic model, with an activation energy (Ea) of 27.280 kJ mol^{-1}. The equilibrium data at all studied temperatures were best described by the Langmuir isotherm model, indicating monolayer adsorption. Thermodynamic analysis revealed negative Gibbs free energy changes ($\Delta G°$) of -24.630, -25.850, -26.810, and -28.550 kJ mol^{-1} at 293, 303, 313, and 323 K, respectively, confirming the spontaneous nature of the adsorption process. The positive enthalpy change ($\Delta H°$ = +12.770 kJ mol^{-1}) indicates that Pb(II) adsorption onto CFA-Dzt is endothermic, while the positive entropy change ($\Delta S°$ = +127.290 J mol^{-1} K^{-1}) suggests increased randomness at the solid–liquid interface during adsorption. This study is limited to the application of CFA-Dzt as an adsorbent. Future work should include a comparative evaluation of the thermodynamic behavior of raw, activated, and immobilized fly ashes to clarify the effects of activation and immobilization on adsorption performance.

References

[1] Arvind Kumar Sharma, Munish Sharma, Simran Sharma, Davendra Singh Malik, Munit Sharma, Munish Sharma, Amit Kumar Sharma, A systematic review on assessment of heavy metals toxicity in freshwater fish species: Current scenario and remedial approaches, *Journal of Geochemical Exploration*, 262, (2024), 107472 https://doi.org/10.1016/j.gexplo.2024.107472

[2] Harsh Sable, Vandana Singh, Vaishali Kumar, Arpita Roy, Soumya Pandit, Kirtanjot Kaur, Sarvesh Rustagi, Sumira Malik, Toxicological and bioremediation profiling of nonessential heavy metals (mercury, chromium, cadmium, aluminium) and their impact on human health: A review, *Toxicologie Analytique et Clinique*, 36, 3, (2024), 205-234 https://doi.org/10.1016/j.toxac.2024.03.096

[3] Habibun Nabi Muhammad Ekramul Mahmud, A. K. Obidul Huq, Rosiyah binti Yahya, The removal of heavy metal ions from wastewater/aqueous solution using polypyrrole-based adsorbents: a review, *RSC Advances*, 6, 18, (2016), 14778-14791 https://doi.org/10.1039/C5RA24358K

[4] Gayatri Pandey, Nitesh Singh Rajput, Umesh Kumar Sharma, Manmohan Singh Chauhan, Narendra Pal Lamba, Remediation of environmental issues using graphene based materials for water purification: Synthesis, kinetics, and factors effecting the removal of heavy metal ions, *Next Materials*, 8, (2025), 100765 https://doi.org/10.1016/j.nxmate.2025.100765

[5] Shreya Kotnala, Shalini Tiwari, Arunima Nayak, Brij Bhushan, Subhash Chandra, Cassio Rocha Medeiros, Henrique Douglas Melo Coutinho, Impact of heavy metal toxicity on the human health and environment, *Science of The Total Environment*, 987, (2025), 179785 https://doi.org/10.1016/j.scitotenv.2025.179785

[6] Vinay Kumar, S. K. Dwivedi, Seungdae Oh, A critical review on lead removal from industrial wastewater: Recent advances and future outlook, *Journal of Water Process Engineering*, 45, (2022), 102518 https://doi.org/10.1016/j.jwpe.2021.102518

[7] Milton Manyangadze, Nyaradzai M. H. Chikuruwo, T. Bala Narsaiah, Ch Shilpa Chakra, Gratitude Charis, Gwiranai Danha, Tirivaviri A. Mamvura, Adsorption of lead ions from wastewater using nano silica spheres synthesized on calcium carbonate templates, *Heliyon*, 6, 11, (2020), https://doi.org/10.1016/j.heliyon.2020.e05309

[8] Hyun-Kyung Kim, So-Jeong Kim, Hye-Ran Kim, Jae-Woo Park, Nitric acid modified powdered activated carbon for simultaneous adsorption of lead and phenol in aqueous solution, *Journal of Environmental Chemical Engineering*, 12, 6, (2024), 114889 https://doi.org/10.1016/j.jece.2024.114889

[9] Rachid El Kaim Billah, Md Aminul Islam, Moonis Ali Khan, Mazen K. Nazal, Lahoucine Bahsis, Mounia Achak, Alaa El Din Mahmoud, Md Abdul Aziz, Byong-Hun Jeon, Adsorption of lead(II) onto magnetic chitosan@calcium phosphate rock biocomposite, *Materials Chemistry and Physics*, 332, (2025), 130249 https://doi.org/10.1016/j.matchemphys.2024.130249

[10] Urwa Mahmood, Ali S. Alkorbi, Tanveer Hussain, Ahsan Nazir, Muhammad Bilal Qadir, Zubair Khaliq, Sajid Faheem, Mohammed Jalalah, Adsorption of lead ions from wastewater using electrospun zeolite/MWCNT nanofibers: kinetics, thermodynamics and modeling study, *RSC Advances*, 14, 9, (2024), 5959-5974 https://doi.org/10.1039/d3ra07720a

[11] Di Zhang, Bo Wu, Tongtong Wang, Murat Yılmaz, Gaurav Sharma, Amit Kumar, Hui Shi, Multi-mechanism synergistic adsorption of lead and cadmium in water by structure-functionally adapted modified biochar: A review, *Desalination and Water Treatment*, 322, (2025), 101156 https://doi.org/10.1016/j.dwt.2025.101156

[12] Bonusa Nabila Huda, Endang Tri Wahyuni, Mudasir Mudasir, Simultaneous adsorption of Pb(II) and Cd(II) in the presence of Mg(II) ion using eco-friendly immobilized dithizone on coal bottom ash, *South African Journal of Chemical Engineering*, 45, (2023), 315-327 https://doi.org/10.1016/j.sajce.2023.06.007

[13] Z. T. Yao, X. S. Ji, P. K. Sarker, J. H. Tang, L. Q. Ge, M. S. Xia, Y. Q. Xi, A comprehensive review on the applications of coal fly ash, *Earth-Science Reviews*, 141, (2015), 105-121 https://doi.org/10.1016/j.earscirev.2014.11.016

[14] Abdallah Dindi, Dang Viet Quang, Lourdes F. Vega, Enas Nashef, Mohammad R. M. Abu-Zahra, Applications of fly ash for CO_2 capture, utilization, and storage, *Journal of CO_2 Utilization*, 29, (2019), 82-102 https://doi.org/10.1016/j.jcou.2018.11.011

[15] Murilo Pereira Moisés, Paula Pomaro de Almeida, Cleiser Thiago Pereira da Silva, Andrelson Wellington Rinaldi, Emerson Marcelo Girotto, Joziane Gimenes Meneguin, Pedro Augusto Arroyo,

Ricardo Eugenio Bazan, Silvia Luciana Fávaro, Eduardo Radovanovic, Synthesis of zeolite from multilayer food packing and sugar cane bagasse ash for CO_2 adsorption, *RSC Advances*, 4, 89, (2014), 48576-48581 https://doi.org/10.1039/C4RA04513K

[16] Richa Soni, Dericks Praise Shukla, Synthesis of fly ash based zeolite-reduced graphene oxide composite and its evaluation as an adsorbent for arsenic removal, *Chemosphere*, 219, (2019), 504-509 https://doi.org/10.1016/j.chemosphere.2018.11.203

[17] Wei Feng, Zhijian Wan, Jacqueline Daniels, Zhikao Li, Gongkui Xiao, Jialin Yu, Dong Xu, Hua Guo, Dongke Zhang, Eric F. May, Gang Li, Synthesis of high quality zeolites from coal fly ash: Mobility of hazardous elements and environmental applications, *Journal of Cleaner Production*, 202, (2018), 390-400 https://doi.org/10.1016/j.jclepro.2018.08.140

[18] Mengfan Gao, Qingliang Ma, Qingwen Lin, Jiali Chang, Hongzhu Ma, Fabrication and adsorption properties of hybrid fly ash composites, *Applied Surface Science*, 396, (2017), 400-411 https://doi.org/10.1016/j.apsusc.2016.10.167

[19] Bonusa Nabila Huda, Endang Tri Wahyuni, Mudasir Mudasir, Eco-friendly immobilization of dithizone on coal bottom ash for the adsorption of lead(II) ion from water, *Results in Engineering*, 10, (2021), 100221 https://doi.org/10.1016/j.rineng.2021.100221

[20] Roohollah Shiralipour, Tooba Hamoule, Keivan Manochehripour, Removal of Pb (II) From Contaminated Water by Bagasse Adsorbent Modified with Dithizone, *Jundishapur Journal of Health Sciences*, 10, 3, (2018), 1-7

[21] Shilpa Yakkerimath, Raviraj M. Kulkarni, Sanjaykumar V. Divekar, Vaibhav R. Chate, Kunkangar Purandara Bekal, Kinetic, adsorption, and thermodynamic study of removal of Cr^{6+} by iron-rich natural clay minerals, *Desalination and Water Treatment*, 318, (2024), 100302 https://doi.org/10.1016/j.dwt.2024.100302

[22] Sania Kanwal, Pooja Devi, Zubair Ahmed, Naveed Ahmed Qambrani, Adsorption isotherm, kinetic and thermodynamic studies for adsorption of fluoride on waste marble powder, *Desalination and Water Treatment*, 319, (2024), 100441 https://doi.org/10.1016/j.dwt.2024.100441

[23] Ping-Hsiu Huang, Chien-Shan Chiu, Wen-Chien Lu, Hu Shao, Po-Hsien Li, Study on activation energy and water adsorption behavior of adzuki beans under different soaking and cooking processing, *Journal of Agriculture and Food Research*, 18, (2024), 101313 https://doi.org/10.1016/j.jafr.2024.101313

[24] Jinfeng Yuan, Weidong Lu, Adsorption of Cr(VI) from aqueous solutions using inorganic clays modified magnetic chitosan adsorbent: Kinetic and thermodynamic study, *Desalination and Water Treatment*, 319, (2024), 100442 https://doi.org/10.1016/j.dwt.2024.100442

[25] Carlos A. Guerrero-Fajardo, Liliana Giraldo, Juan Carlos Moreno-Pirajan, Isotherm, thermodynamic, and kinetic studies of dye adsorption on graphene oxides with varying oxidation degrees, *Results in Engineering*, 26, (2025), 104558 https://doi.org/10.1016/j.rineng.2025.104558

[26] Abhigith Nair, Yogesh Kumar Kumawat, Sonal Choudhary, Jyotendra Nath, Kashma Sharma, Tanveer Rasool, Vishal Sharma, Vijay Kumar, Malachite green dye adsorption from wastewater using pine gum-based hydrogel: Kinetic and thermodynamic studies, *Journal of Molecular Structure*, 1295, (2024), 136671 https://doi.org/10.1016/j.molstruc.2023.136671

[27] Charuta Waghmare, Sujesh Ghodmare, Khalid Ansari, Faisal M. Alfaisal, Shamshad Alam, Mohammad Amir Khan, Yassine Ezaier, Adsorption of methylene blue dye onto phosphoric acid-treated pomegranate peel adsorbent: Kinetic and thermodynamic studies, *Desalination and Water Treatment*, 318, (2024), 100406 https://doi.org/10.1016/j.dwt.2024.100406

[28] Dina Fitriana, Mudasir Mudasir, Dwi Siswanta, The Modification of Coal Fly Ash Adsorbent Using Dithizone Immobilization for Cd(II) Ions Removal, *Jurnal Kimia Sains dan Aplikasi*, 28, 4, (2025), 215-224 https://doi.org/10.14710/jksa.28.4.215-224

[29] Mireia Grivé, Cristina Domènech, Vanessa Montoya, David García, Lara Duro, *Determination and assessment of the concentration limits to be used in SR-Can*, Swedish Nuclear Fuel and Waste Management Co., , Stockholm (Sweden), 2006

[30] Takahiro Yoshida, Tetsuji Yamaguchi, Yoshihisa Iida, Shinichi Nakayama, XPS Study of Pb(II) Adsorption on γ -Al_2O_3 Surface at High pH Conditions, *Journal of Nuclear Science and Technology*, 40, 9, (2003), 672-678 https://doi.org/10.1080/18811248.2003.9715405

[31] Jinhui Huang, Fang Yuan, Guangming Zeng, Xue Li, Yanling Gu, Lixiu Shi, Wenchu Liu, Yahui Shi, Influence of pH on heavy metal speciation and removal from wastewater using micellar-enhanced ultrafiltration, *Chemosphere*, 173, (2017), 199-206 https://doi.org/10.1016/j.chemosphere.2016.12.137

[32] Şeyda Taşar, Ahmet Özer, A Thermodynamic and Kinetic Evaluation of the Adsorption of Pb(II) Ions Using Peanut (*Arachis Hypogaea*) Shell-Based Biochar from Aqueous Media, *Polish Journal of Environmental Studies*, 29, 1, (2020), 293-305 https://doi.org/10.15244/pjoes/103027

[33] Agustino Zulys, Leni Andriyani, Rizkha Fadhilla, Nasruddin Nasruddin, Takuya Mabuchi, Adawiah, Yulyani Nur Azizah, One-pot synthesis of A novel metal organic framework-modified TiO_2@Cr-PTC-HIna as adsorbent for Pb^{2+} removal in aqueous system, *Case Studies in Chemical and Environmental Engineering*, 10, (2024), 100829 https://doi.org/10.1016/j.cscee.2024.100829

[34] Thanooja Nizam, K. Anoop Krishnan, Aruna Joseph, Renju R. Krishnan, Isotherm, kinetic and thermodynamic modelling of liquid phase adsorption of the heavy metal ions Zn(II), Pb(II) and Cr(VI) onto $MgFe_2O_4$ nanoparticles, *Groundwater for Sustainable Development*, 25, (2024), 101120 https://doi.org/10.1016/j.gsd.2024.101120

[35] Bonusa Nabila Huda, Endang Tri Wahyuni, Yuichi Kamiya, Mudasir Mudasir, Kinetic and thermodynamic study on adsorption of lead(II) ions in water over dithizone-immobilized coal bottom ash, *Materials Chemistry and Physics*, 282, (2022), 126005

https://doi.org/10.1016/j.matchemphys.2022.126005

[36] Kousar Yasmeen, Sadia Nawaz, Azhar Iqbal, Asma Siddiqui, Abdul Rehman Umar, Haji Muhammad, Maryam Shafique, Faheem Shah, Sobia Tahir, Abdul Majeed Khan, Muhammad Masab, Muddasir Hanif, Removal of Pb(II) from water samples using surface modified core/shell CdZnS/ZnS QDs as adsorbents: Characterization, adsorption, kinetic and thermodynamic studies, *Arabian Journal of Chemistry*, 15, (2022), 104224 https://doi.org/10.1016/j.arabjc.2022.104224

[37] Ebuka Chizitere Emenike, Hussein K. Okoro, Ghadah M. Al-Senani, Salhah D. Al-Qahtani, Kingsley O. Iwuozor, Abel U. Egbemhenghe, Joshua Emeghai, Adewale George Adeniyi, Adsorptive removal of Cr(VI) and Pb(II) using biochar from biomass and plastic waste: characterization and performance evaluation, *Biomass and Bioenergy*, 207, (2026), 108722 https://doi.org/10.1016/j.biombioe.2025.108722

[38] Jingyi Chen, Xiaoxue Zhang, Junsheng Liu, Shan Jiang, Chunyu Ji, Jie Zhang, Preparation of polyethyleneimine/graphene oxide membranes and their adsorptions for Pb(II), Cu(II) and Zn(II) in mixed systems, *Desalination and Water Treatment*, 322, (2025), 101099 https://doi.org/10.1016/j.dwt.2025.101099

[39] Naser Samadi, Reza Hasanzadeh, Mohamad Rasad, Adsorption isotherms, kinetic, and desorption studies on removal of toxic metal ions from aqueous solutions by polymeric adsorbent, *Journal of Applied Polymer Science*, 132, 11, (2015), https://doi.org/10.1002/app.41642